Giant Bandgap Renormalization and Exciton-Phonon Scattering in Perovskite Nanocrystals

Rinku Saran, Amelie Heuer-Jungemann, Antonios G Kanaras, and Richard J Curry**

Dr R. Saran, Prof R.J. Curry
The Photon Science Institute, School of Electrical and Electronic Engineering, The University of Manchester, Alan Turing Building, Oxford Road, Manchester, M13 9PL, United Kingdom.
E-mail: rinku.saran-2@manchester.ac.uk; richard.curry@manchester.ac.uk

Dr A. Heuer-Jungemann, Prof A.G. Kanaras
Physics and Astronomy, Faculty of Physical Sciences and Engineering, University of Southampton, Southampton, SO17 1BJ, United Kingdom.

Keywords: cesium lead halides, perovskites, nanocrystals, exciton-phonon interactions, bandgap renormalization

Abstract

Understanding the interactions between photoexcited charge carriers (electrons and holes) with lattice vibrations (phonons) in quantum confined semiconductor nanocrystals (NCs) is of fundamental interest and a prerequisite for their use in fabricating high-performance optoelectronic devices. Such interactions have a significant impact on their optoelectronic properties including their charge carrier mobility and photoluminescence. Here, we investigate these interactions in cesium lead halide ($CsPbX_3$, where X is Cl, Br or I) NC perovskites. We show that a wide broadening of the excitonic linewidth in these NCs arises from strong exciton-phonon coupling, which is substantially dominated by longitudinal optical phonons via the Fröhlich interaction. Unlike the behavior of conventional semiconductors these NCs display a general red-shift of their emission energy peak with reducing temperature. Interestingly, the $CsPbCl_3$ NCs also display an initial blue-shift and undergo at structural phase transition at ~175 K to 200 K. The anomalous red-shift observed is modeled and analyzed using a Bose-Einstein two-oscillator model to interpret the interaction of excitons with acoustic and optical phonons which induce a renormalization of the bandgap. The net renormalization due to zero point motion (T= 0 K) was found to be ~41.6 meV and ~94.9 meV for $CsPbBr_3$ and $CsPbI_3$ NCs respectively.

1. Introduction

Semiconductor colloidal nanocrystals (NCs), wherein the NC dimensions are comparable to the de Broglie wavelength of the charge carriers, have attracted considerable interest during the past decade as they exhibit size tunable optoelectronic properties due to quantum confinement. Fundamental studies of their properties have led to their successful application in a variety of devices including photovoltaic cells,[1] photodetectors[2] and light emitting diodes.[3] A new addition to the library of semiconductor NCs are the recently reported cesium lead halide perovskites ($CsPbX_3$, where X is Cl, Br or I).[4] Like other types of semiconductor NC, one of their most compelling optical properties is their size-tunable photoluminescence (PL) across the entire visible (400-700 nm) spectrum and beyond into the near infrared (NIR). This can be achieved chemically through control of the halide ion, and also via varying the NC size below the bulk exciton Bohr diameter ($CsPbCl_3$ ~5 nm, $CsPbBr_3$ ~7 nm and $CsPbI_3$ ~12 nm).[4] In addition, they display a narrow and bright emission with PL quantum yields of ~80-90% leading to their recent use in light emitting devices[5] and the demonstration of amplified spontaneous emission.[6] Though, as recently reported, their poor performance in light emitting device applications originates from an efficient bi-exciton interaction meaning further work is required.[7] To date, the majority of the reported work on these NCs has focused on their synthesis and device applications. Recently, attention has turned to study their quantum confined optical properties including the investigation of the origin of their high PL quantum yields.[7-9]

The choice of semiconductor material for use in an optoelectronic device is principally based on its bandgap energy and the device performance is governed by the nature of photogenerated excited states: their binding energy or diffusion length, interaction with phonons and their relaxation or charge carrier extraction mechanism. In both bulk hybrid organic–inorganic perovskites (e.g. methylammonium/formamidinium - $MA/FAPbX_3$) and inorganic $CsPbX_3$ perovskites, the anomalous red-shift of bandgap energy with the reduction in temperature[10-12] and also the nature of excited carriers is unclear and often argued.[13] Recent insight into hybrid perovskites on their underlying physics through temperature dependent studies of PL emission has been reported,[10, 11, 13-16] though the origin of the red-shift of their bandgap energy is still not fully understood.[17] Unlike bulk semiconductors the interactions of NC excited states with phonons are still to be resolved. Early theoretical studies predicted that electron-phonon coupling is suppressed in NCs due to the discrete nature of their electronic states whose energy separation exceeded the longitudinal-optical (LO) phonon energy by an order of magnitude.[18-21] Also, the interaction of longitudinal-acoustic (LA) phonons with the deformation potential, which is weak in the bulk, was predicted to weaken further with reduction in NC size. Surprisingly, deviations from these predictions were observed by experimental studies on NCs. For example, strong electron-phonon coupling in a variety of NCs systems has been observed (e.g. PbS[22], CdSe[23] and PbSe[24]), with energy-dissipation rates of the order of ~0.1-10 eV/ps[18, 24] and which increase with the increase in NC size.[24] Intraband carrier relaxation in NCs is also found to occur on femtosecond to picosecond time scales,[23, 25] and a strong

interaction between the excitons and acoustic phonons have also been observed.[22, 23] Very recently, significant insight has been provided in this context through a combination of *ab initio* simulation studies and inelastic neutron scattering experiments on PbS NCs.[22] The study revealed that unlike in bulk crystals, where electronic transitions mainly occur via high energy optical phonon interactions, in NCs a high density (~200) of low energy acoustic phonons (from Pb surface atoms) are also heavily involved that drive multi-phonon transitions. Additionally, it was observed that the phonon density of states and mean square displacement of atoms were not modified by a change in NC size.

With the recent emergence of all inorganic $CsPbX_3$ NCs for light emitting devices it is of great interest to study the temperature dependence of their optical properties and in particular PL emission. Here, we therefore investigate exciton-phonon interactions in these NCs via examining their steady-state PL emission spectra measured over a range of temperatures (T = 300 K-5 K). In doing so, we elucidate the photophysics of their excited states, thermal broadening of their PL emission, and the anomalous red-shift of their bandgap with decreasing temperature.

2. Result and Discussion

$CsPbX_3$ NCs were synthesized following a previously reported experimental procedure as described in the Supporting Information.[4] The room temperature optical absorption and PL emission spectra, representative TEM images of the cubic shaped NCs, and the size distribution of $CsPbX_3$ NCs are shown in **Figure 1**a, b and c, respectively. All three NC types display visible excitonic absorption features owing to the quantum confinement of carriers. Extended range absorption spectra along with their second derivatives are provided in Supporting Information Figure S1. The optoelectronic properties of crystalline solids are predominantly governed by their crystal structure and constituent atoms. The perovskite $CsPbX_3$ crystal forms an octahedral quasi-complex $Pb^{2+}(X^-)_6$ embedded in a simple cubic matrix of Cs^+ cations as shown schematically inset to **Figure 2**a. The electronic density of states of $CsPbX_3$ crystals have been previously reported, obtained using the linear combination of atomic orbitals (LCAO)[26, 27] method and more recently using an *ab initio* approach.[4] The former model reveals that the upper valence band state is of a mixed character of halide *n*p and Pb^{2+} (6s) orbitals whilst the latter reveals that valence band state is predominantly formed from halide ion states (Cl^- (3p), Br^- (4p) and I^- (5p)), with both models predicting the lower conduction band arising from Pb^{2+} (6p) states. A direct bandgap minimum is found at the R-point in the Brillouin zone that is two-fold spin degenerate.[8] The first exciton peak (R-point exciton) in the absorption could therefore arise from a halide *n*p to Pb^{2+} 6p transition.

The photoluminescence excitation (PLE) spectra of the $CsPbX_3$ NCs are shown in Figure 1d displaying the PL intensity dependence on the excitation energy. The spectra closely follow the absorption spectra of the NCs overlapping with the strong features observed in the absorption (Supporting Information Figure S1). It can be seen that both the low and high energy ('hot') excited carriers are efficiently channeled to the emitting energy states of the NCs reflecting the high oscillator

strength of the transitions.[8] Furthermore, the PL emission intensity significantly increases as the excitation energy is increased from the absorption edge and is accompanied by a small blue-shift. It is noted that the $CsPbI_3$ PL emission intensity is then reduced again at the highest excitation energies used (~300 nm). which may also occur for the other NCs in the spectral region beyond our measurement capability. The small blue shift at relatively high energy excitation is attributed to the size distribution of NCs which is directly correlated with the confined energy of the emissive state. For $CsPbI_3$ maximum PL intensity is observed when exciting at ~355 nm and ~460 nm corresponding to the higher energy states observed in the absorption spectra. At wavelengths below 340 nm the excitation energy (hv) becomes greater than twice the $CsPbI_3$ bandgap (E_g), the lowest threshold value for multiple exciton generation (MEG), which may be expected in $CsPbX_3$ NCs due to similar and small effective mass of the electron and hole.[4, 28] However, PLE spectra shows that the excess energy when exciting in this region is lost through non-radiative processes with reduced emission intensity of the lower energy PL. Time resolved PL lifetime decay of the $CsPbX_3$ NCs revealing the exciton decay dynamics in NCs is shown in Figure 2b. The NCs display a bi-exponential PL decay behavior with lifetimes of ~2.4 ns and ~14 ns for $CsPbBr_3$ and ~4.5 ns and ~29.4 ns for $CsPbI_3$ with each component having relative amplitudes of (~ 0.92 and ~0.08) and (~0.52 and ~0.48), respectively. The lifetime of the both these NCs at room temperature have been measured previously[4, 8] and agree well with the reported values. The PL decay lifetime of the $CsPbCl_3$ NCs was found to be faster than our system response and could not be obtained.

The exciton-phonon interactions in $CsPbX_3$ NCs are examined by measuring their PL emission spectra over the temperature range T = 300 K to 5 K as shown in Figure 2c. Each spectrum was fitted using a Gaussian curve enabling the extraction of the FWHM and PL peak energy position. The temperature dependent broadening of the PL is mainly due to lattice vibrations in a crystal that perturb the motions of electrons in different ways defined as the deformation potential, piezoelectric and the Fröhlich interaction. The deformation potential interaction is interpreted as the interaction of an electron with optical or acoustic phonons, as if crystal atoms are displaced from their equilibrium positions analogous to a homogenously strained crystal. Such an interaction can severely influence the electronic band structure. In crystals not having a center of symmetry the electric field induced by the strain may also lead to the interaction of acoustic phonons with electrons via the piezoelectric effect. Unlike the strain induced interaction, the Fröhlich interaction is a Coulombic interaction, it describes the interaction of electron with longitudinal electric field created by LO phonon mode due to the displacement of oppositely charged out-of-phase atoms.[29] These interactions vary with temperature due to their dependence on the phonon population and consequently influence the PL emission. Within the first order perturbation theory the overall PL emission broadening of the lowest-lying 1S exciton state $\Gamma(T)$ can be described by sum of three types of broadening contribution given by Segall's expression,[30] and in the case of the presence of any ionized impurities an additional term can be added[31, 32] to the expression to give:

$$\Gamma(T) = \Gamma_{inh} + \Gamma_{AC} + \Gamma_{LO} + \Gamma_{imp} \quad (1)$$

$$\Gamma(T) = \Gamma_{inh} + \varphi_{AC}T + \frac{\varphi_{LO}}{e^{(\omega_{LO}/kT)}-1} + \varphi_{imp}e^{-\langle E_b\rangle/kT} \quad (2)$$

where Γ_{inh} is the inhomogeneous broadening constant which arises from scattering due to exciton-exciton and crystal disorder, and is temperature independent. In the second term (Γ_{AC}) φ_{AC} represents an exciton-acoustic phonon coupling coefficient, mainly relating to the deformation potential interaction which is linearly dependent on temperature. In the third term (Γ_{LO}) φ_{LO} is the exciton-longitudinal optical phonon coupling coefficient or the Fröhlich coupling coefficient which is associated with the Bose–Einstein distribution of the LO phonons given as $1/(e^{(\omega_{LO}/kT)} - 1)$. Here ω_{LO} is the energy of the LO phonons, *k* is Boltzmann's constant and *T* is the temperature. In the final impurity term (Γ_{imp}) φ_{imp} is the linewidth arising due to scattering from fully ionized impurities which is governed by their average binding energy $\langle E_b\rangle$. The PL emission FWHM of the $CsPbX_3$ NCs are plotted in **Figure 3**a-c along with best fits obtained via least square fitting using the Equation (1). The parameters derived via fitting are presented in **Table 1**. The individual contribution to broadening arising from acoustic and optical phonons interactions and due to the presence of any impurity states is also plotted for each NC type (right axis). It can be seen that the FWHM has a significant temperature dependence implying strong exciton-phonon interactions in these NCs. This leads to wide thermal broadening of emission as the temperature is increased from 5 K to 300 K of ~33.53 meV, ~51.5 meV and ~34.96 meV for $CsPbCl_3$, $CsPbBr_3$ and $CsPbI_3$, respectively.

For $CsPbCl_3$ NCs the PL broadening is dominated by LO phonons in the high temperature regime followed by a crossover between the acoustic and LO phonons as the temperature is further decreased so that acoustic phonon interactions then govern the broadening, Figure 3a. For the majority of semiconductors[30] acoustic phonons typically dominate for T ≤ 80 K as the LO phonon population is significantly reduced in this temperature range. In semiconductors like GaN and ZnS, acoustic phonons solely contribute up until T~120 K, and a crossover between phonon contributions is observed at T ~220 K for GaN.[33, 34] Attempts to fit the $CsPbBr_3$ PL FWHM on the same basis did not provide a good fit, however setting ($\varphi_{AC} = 0$) yielded an LO phonon energy ~2.25 meV. This value is significantly smaller than previous reports for a wide variety of NC material systems and perovskites (~10-90 meV, Supporting Information Table 1) and results from the observed pseudo-linear behavior of the FWHM down to very low temperatures (~20 K). The inclusion of the impurity scattering term in Equation (2) enables a good fit with ($\varphi_{AC} = 0$), though addition of the acoustic term significantly improves fitting in the range of T≤ 50 K. Thus the fit for the entire temperature range can be obtained by including the acoustic contribution determined via fitting the low temperature (T≤ 50 K) regime. This provides very good fit to the experimental data with coefficient of determination (R^2 >0.999) as shown in Figure 3b. We note that previously in bulk $CsPbBr_3$ a very similar pseudo-linear behavior of the FWHM has been observed from room temperature down to ~20 K and attributed to the presence of

defect states that arise due to Pb^{+2} or Br^{-1} vacancies.[35] Others have reported that optimal growth conditions are required for each halide identity in perovskites and that they should be Pb^{+2} rich for Cl and Br and Pb^{+2} poor for I to avoid such vacancy defects.[36] With Br NCs laying between these two extremes it may be more susceptible to defect or impurity incorporation in non-optimal growth conditions. The presence of such states have a noticeable impact on PL broadening as seen in the Figure 3b which is larger than the LO phonon contribution. Strong contribution from impurities to the linewidth broadening is rarely observed in NCs. For quantum well systems,[32] it has been reported that an impurity contribution is almost negligible for impurity concentrations of below $10^{-15}cm^{-3}$, though such behavior may also arise due to exciton localization. Here, a crossover between acoustic and LO phonon contribution occurs at T~190 K whilst contribution from the impurity scattering contributes down to T~20 K. For $CsPbI_3$ NCs, LO phonons significantly dominate over the acoustic and for T≤60 K the LO phonon contribution becomes negligible and the relatively small broadening is purely due to acoustic phonon scattering. The broadening of the $CsPbI_3$ NC PL may be fitted without the inclusion of the impurity term with LO phonon interaction dominating for T > 90 K, Figure 3c.

We can conclude that exciton-phonon coupling in $CsPbX_3$ NCs leads to broadening of PL emission and the dominant contribution ($CsPbCl_3$ ~20.6 meV, $CsPbBr_3$ ~19.1 meV and $CsPbI_3$ ~26.2 meV) arises due to Fröhlich type carrier interaction with LO phonons. Acoustic phonons also contribute to the broadening though their contribution is smaller ($CsPbCl_3$ ~12.8 meV, $CsPbBr_3$ ~9.8 meV and $CsPbI_3$ ~7.2 meV) though significant in the low temperature regime. For $CsPbBr_3$ scattering due to impurities leads to additional broadening of PL ~23.4 meV. The LO phonon energies for $CsPbX_3$ NCs (X = Cl ~42.8 $\pm$ 4.5 meV, Br ~44.4 $\pm$ 10.2 meV and I ~26.3 $\pm$ 7.0), that depend on the inverse of square root of atomic mass of the respective halide ion, were found to be greater or equivalent to the thermal energy at 300 K (~ 25 meV). As such, at high temperatures, the lowest lying exciton can absorb one LO phonon via the Fröhlich interaction with energy ω_{LO}. Subsequently, it may either scatter within the same bound state (intraband) or with discrete excitonic states, and can also dissociate into free charge carriers.[37] These processes are governed by their respective exciton binding energies (E_b^{ex}) which are reported as ($CsPbCl_3$ ~75 meV, $CsPbBr_3$ ~40 meV and $CsPbI_3$ ~20 meV).[4] The higher value of E_b^{ex} for $CsPbCl_3$ indicates that the excitons are highly stable even at room temperature ($E_b^{ex} > \omega_{LO} > kT$). For $CsPbBr_3$ and $CsPbI_3$ E_b^{ex} is similar to ω_{LO} thus the probability for their dissociation is not high, in particular at temperatures T < 300. It is interesting to compare the values of the parameters derived in these NCs with those of bulk $CsPbX_3$, ($MA/FAPbX_3$)[38,39] and other semiconductors (Supporting Information Table 1). The LO phonon energies obtained for $CsPbX_3$ NCs are close to previously obtained reported values for bulk crystals [$CsPbCl_3$ (~43 meV and ~46.49 meV)[12, 40] ; $CsPbBr_3$ (~47.3 meV and 47.4 meV)][35] obtained via PL and Raman studies, respectively. These, phonon energies are significantly higher than found for hybrid perovskites ($MAPbCl_3$ ~27.9 meV, $MAPbBr_3$/$FAPbBr_3$ ~15.3 meV and MA/FA-PbI_3 ~11.5 meV)[38,39] which lie within the range of other semiconductor NC systems (e.g. CdSe, ZnSe, GaAs, CdS and ZnS). The Fröhlich coupling

coefficient (φ_{LO}) that depends on the exciton binding energy and the polarity of the semiconductor were found to be ($CsPbCl_3$ ~87.2 $\pm$ 14.9 meV, $CsPbBr_3$ ~86.7 $\pm$ 31.4 meV and $CsPbI_3$ ~46.3 $\pm$ 11.1). The values obtained for φ_{LO} are also in the range of $MAPbBr_3$/$FAPbBr_3$ ~60 meV and $MAPbI_3$/$FAPbI_3$ ~40 meV.[38] For $CsPbCl_3$ and $CsPbBr_3$ φ_{LO}~ 88 meV which is larger than found for systems having similar LO phonon energies and is close to that found for ZnSe and $CH_3NH_3PbI_{3-x}Cl_x$ (Supporting Information Table 1). The low value of φ_{LO} and ω_{LO} together with low E_b^{ex} implies that excitons in $CsPbI_3$ have higher probability to dissociate and thus are well suited for photovoltaic and photodetector applications.

The temperature dependence of the PL peak energy of $CsPbX_3$ NCs are shown in **Figure 4**a-c, displaying a red-shift with reducing temperature for $CsPbBr_3$ and $CsPbI_3$ NCs in agreement with studies of the bulk perovskites.[11, 12] The magnitude of the observed red-shift between 300 K and 5 K for the $CsPbBr_3$ and $CsPbI_3$ NCs is ~29.7 meV and ~49.6 meV at respective average rates of ~100 μeV/K and ~168 μeV/K. The PL of the $CsPbCl_3$ NCs displays a similar red-shift (~10 meV) as the temperature is reduced below 175 K (at a rate of ~58.82 μeV/K) though prior to reaching this temperature a similar magnitude blue-shift of ~7 meV is seen. This temperature dependent change from an initial blue-shift to a red-shift is attributed to a phase change in the crystal structure. Bulk $CsPbCl_3$ is known to undergo four structural phase changes within the temperature range of 330 K to 310 K, and a fifth phase change (loss of a center of symmetry) is reported to occur in the temperature range of T = 180 K - 200 K.[41-43] Experiments repeated on different samples displayed similar behavior confirming that this is a temperature induced phase change corresponds to the change in PL peak energy (Supporting Information Figure S3). It implies that the NC structure plays a central role in determining the nature of the PL temperature dependence in these systems. Interestingly, the observation of the significant red-shift of the PL emission peak in $CsPbX_3$ NCs with decreasing temperature contrasts the behavior typically found in conventional semiconductors in which a blue-shift is observed. Literature reports of such observation is limited to a small group of materials that includes black phosphorus,[44] bulk perovskites ($CH_3NH_3PbX_3$, $CsSnX_3$ and $CsPbX_3$),[10, 12, 16, 45] lead salts (PbS, PbSe and PbTe)[46-48] and cuprous halides (CuCl, CuBr and CuI).[49]

Over the past few decades the observed change in the bandgap energy with temperature have been modeled by using various empirical formulas such as the widely used Varshni model.[50] Several other models based on theoretical foundation have also been proposed by O'Donnell[51] and Pässler.[52] However, the anomalous temperature dependence of bandgap is still puzzling and therefore exploring novel materials that exhibit similar behavior is interesting and helpful in providing deeper insight. Within the quasi-harmonic approximation, the overall change in the bandgap energy of a semiconductor with the change in temperature $\left(\frac{\partial E_g}{\partial T}\right)$ can be expressed as:[45]

$$\frac{\partial E_g}{\partial T} = \left(\frac{\partial E_g}{\partial V}\right)\left(\frac{\partial V}{\partial T}\right) + \sum_{j,\vec{q}}^{N}\left(\frac{\partial E_g}{\partial n_{j,\vec{q}}}\right)\left(n_{j,\vec{q}} + \frac{1}{2}\right) \qquad (3)$$

The first component in Equation (3), $\left(\frac{\partial E_g}{\partial V}\right)\left(\frac{\partial V}{\partial T}\right)$, describes the contribution from the expansion of the lattice to the change in bandgap energy, given by the product of hydrostatic deformation potential $\left(\frac{\partial V}{\partial T}\right)$ for an expansion coefficient $\left(\frac{\partial E_g}{\partial V}\right)$. The expansion coefficient for a given semiconductor can either be positive or negative. For example, in cesium tin halide ($CsSnX_3$) it has been shown that the bandgap decreases with the lattice constant.[53] This then further decreases upon reduction of the sample temperature and dominates over electron-phonon interactions.[45, 53] The change in bandgap energy due to the electron-phonon interaction is described by the second perturbative component in the Equation (3). In practice, it is difficult to calculate the coefficient $\left(\frac{\partial E_g}{\partial n_{j,\vec{q}}}\right)$ as this requires summation over all phonon modes with full pseudo-potential description of electronic bands of semiconductor and remains a challenging task. This imposes onerous restrictions on the precise calculation and analysis of the temperature dependent bandgap variation due electron-phonon interactions. To circumvent this problem efforts have been made theoretically to take into account the coefficient $\left(\frac{\partial E_g}{\partial n_{j,\vec{q}}}\right)$ in order to analyze experimental data, for example via using the Bose-Einstein oscillator model.[46, 49, 54, 55] Here, we use a Bose-Einstein two-oscillator model to analyze the anomalous behavior in $CsPbX_3$ NCs. The model used only considers the contribution of acoustic and optical modes, instead of summing all the possible phonon modes in the Brillouin zone, and relies on the fact that the two oscillators give electron-phonon contributions of opposite signs. The sign difference stems from the fact that a relatively large mass difference between the constituent atoms (i.e. Pb ~207.2 and Cl ~35.45, Br ~79.9 and I ~129.9) lead to a formation of an energy gap in the phonon dispersion branches. Thus the lattice dynamics requires a bandgap renormalization of the distribution of density of phonons of lead and halides. Hence, the electronic energy $E_n(\vec{k})$ of a band *n* can be given by sum of the un-renormalized unperturbed band energy $\epsilon_n(\vec{k})$ and a perturbation as:[49]

$$E_n(\vec{k}) = \epsilon_n(\vec{k}) + \sum_{j,\vec{q}}^{N}\left(\frac{\partial E_n(\vec{k})}{\partial n_{j,\vec{q}}}\right)\left(n_{j,\vec{q}} + \frac{1}{2}\right) \qquad (4)$$

The second component in Equation (4) represents the summation of *N* phonon modes of electron-phonon coupling energies of $\left(\frac{\partial E_n(\vec{k})}{\partial n_{j,\vec{q}}}\right)$, where $n_{j,\vec{q}}$ is the phonon occupation number (average phonon density at energy $\hbar\omega_{j,\vec{q}}$) in the phonon branch *j*, with a wave vector $\vec{q}$ that follows the Bose-Einstein distribution as $n_{j,\vec{q}} = \frac{1}{(e^{\hbar\omega_{j,\vec{q}}/kT}-1)}$. Here, $\hbar$ is the reduced Plank's constant, $\omega_{j,\vec{q}}$ is the angular frequency of phonon mode, *k* is Boltzmann's constant and *T* is the temperature. The first term $\left(\frac{\partial E_n(\vec{k})}{\partial n_{j,\vec{q}}}\right)$ in the component represents Debye-Weller and Fan[56] (real part of self-energy) terms and the second term $\left(n_{j,\vec{q}} + \frac{1}{2}\right)$ phonon occupation number. Both Debye-Weller and Fan terms arise from perturbation theory of up to second order.[57] The Debye-Weller term is related to the simultaneous interaction of an electron with two phonons in the branch *j* having the wave vector $\vec{q}$ which is

calculated using first-order perturbation theory. The Fan term (self-energy) describes the interaction of an electron with one phonon (emission and re-absorption of one phonon or vice-versa). The self-energy is a complex function with the real part describing the energy shift and the imaginary part describing the broadening (i.e. the FWHM) of the renormalized state.[58] The imaginary part of the self-energy vanishes at the uppermost valence band state and at the lowest conduction band state, which is typically observed as a sharp absorption or emission corresponding to those states at low temperatures. Equation (4) can be approximated to model the behavior for N = 2 phonon modes (acoustic and optical) of electron-phonon coupling energies of $\left(\frac{\partial E_g}{\partial n_{j,\vec{q}}}\right)$ represented by electron-phonon coupling coefficient and their atomic mass as:[49]

$$E_0(T,M) = E_0 + \frac{A_{ac}}{M_{ac}\omega_{ac}}\left(\frac{1}{e^{\omega_{ac}/kT}-1}+\frac{1}{2}\right) + \frac{A_{opt}}{M_{opt}\omega_{opt}}\left(\frac{1}{e^{\omega_{opt}/kT}-1}+\frac{1}{2}\right) \qquad (5)$$

where, E_0 is unrenormalized bandgap energy, A_{ac} and A_{opt} represent the relative weight of oscillators (or the electron-phonon coupling coefficients), ω_{ac} and ω_{opt} are the acoustic and optical phonon energies, and M_{ac} and M_{opt} are the atomic masses of the oscillator. Previously for $CsSnI_3$ perovskite it has been shown that contribution of acoustic and optical modes cancel out each other,[45] as such their bandgap energy decreases linearly with decrease in temperature and follows $\left(\frac{\partial E_g}{\partial V}\right)\left(\frac{\partial V}{\partial T}\right)$, equation (3).

As seen in Figure 4b and 4c the model provides an excellent fit (solid line) to the experimental data obtained for $CsPbBr_3$ and $CsPbI_3$ NCs across the temperature range studied. The values of the derived parameters are presented in Table 2. The relative contributions of exciton coupling with acoustic and optical phonon branches, and the un-renormalized bandgap energy (right axis) are also plotted. It can be seen that both acoustic and optical phonons are heavily involved in the NC's electronic transitions and oppose each other, with the former resulting in a red-shift whilst the later causes the blue-shift of the PL peak energy. The acoustic mode displays a linear dependence with temperature which clearly indicates that the phonon energy of these modes in respective NCs is less than (kT ~25 meV) and follows $\left(\frac{1}{e^{\omega_{ac}/kT}-1} \approx \frac{kT}{\omega_{ac}}\right)$ whilst optical modes display temperature dependence that follows the Bose-Einstein distribution. The acoustic mode vibrations are dominated by the displacement of heavy Pb atoms with phonon energy of ω_{ac} (purely Pb-like phonons), whilst optical mode are dominated by displacement of light halogen atoms with phonon energy of ω_{opt} (purely X-like phonons, X = Br, I). As the temperature is reduced below 300 K the optical phonon interaction tends to increase the band gap, though simultaneously the phonon population (and therefore the strength of this interaction) is decreasing which leads to the acoustic mode's dominance. When the temperature reaches 50 K and 75 K for Br and I respectively, the optical phonon contribution becomes constant, thus beyond these temperatures the overall change in the bandgap energy arises due to the acoustic mode interaction which sharply decreases the bandgap energy below these temperatures. The overall increase in bandgap due to optical phonons (Br ~ 22.4 meV and I ~ 36.8 meV) is considerably less than the decrease due to acoustic phonons Br ~52.4 meV and I ~ 86.3

meV. The acoustic phonon energies obtained using this model were for $CsPbBr_3$ ~ 3.42 meV and $CsPbI_3$ ~ 6.27 meV. Likewise, the energy of optical phonons obtained was for $CsPbBr_3$ ~ 41.87 meV which is close to energy of LO phonons obtained via analysis of their PL FWHM. For $CsPbI_3$ the values obtained from the fitting is ~ 49.53 meV which is almost double the value of their LO phonon energy found from the FWHM fitting. This suggest involvement of another I-like band, as in iodide perovskites ($MAPbI_3$) strong LO-TO (transverse optical) splitting is found[39] which may also account for the relatively higher acoustic phonon energies seen in $CsPbI_3$ NCs. The obtained values of unrenormalized bandgap energy are ~ 2.4 eV and ~ 1.8 eV for $CsPbBr_3$ and $CsPbI_3$, respectively. Within the framework of two-oscillator model, the bandgap renormalization at T= 0 K in $CsPbX_3$ NCs can thus be obtained as both the lattice constant and electron-phonon interactions vary as the inverse of square root of atomic mass of the constituent atom.[46, 49] The net bandgap renormalization due to zero-point motion can be obtained via extrapolation to T = 0 K. The renormalization due to zero point motion of Pb atoms is found to be ~3.7 meV and ~11.85 meV in $CsPbBr_3$ and $CsPbI_3$ respectively. The corresponding renormalization due to the halogen atoms is ~ 45.3 meV for Br and ~106.7 meV for I with respect to E_0 resulting in a net renormalization of ~41.6 meV and ~94.86 meV for the respective systems. The net renormalization at T=0 observed here for $CsPbI_3$ NCs is significantly larger than that reported previously for materials displaying similar anomalous behavior (lead slats and cuprous halides). For PbS crystals and CuI the net renormalization was found equal to zero, though the isotopic substitution of S in PbS (i.e. increasing the S mass) resulted in renormalization energy of 29 meV. Furthermore, size dependent studies on PbS and PbSe crystals has revealed that for very small size NCs such an anomalous behavior disappears in PbS NCs (e.g. for d ~ 2.8 nm) and in the case of PbSe NCs (d~2.3 nm) even displays the opposite behavior (a blue-shift). These collective results suggests that both atomic mass and NC size in such material systems can have a significant effect on bandgap energy and opens future prospect to study $CsPbX_3$ NCs as a function of their crystal size.

3. Conclusions

To summarize, we have conducted an in-depth study to quantify exciton-phonon interactions in $CsPbX_3$ NCs that have a direct consequence on their intrinsic optical and electronic properties. Our analysis of temperature dependent PL data provides evidence that LO phonon scattering via the Fröhlich interaction mainly responsible for thermal broadening of exciton linewidth in these NCs. However, acoustic phonon scattering dominates at low temperatures though with an additional more dominant contribution in the case of $CsPbBr_3$ due to the presence of ionized impurities. The distortion induced due to optical phonons is typically microscopic in nature and within the primitive cell and are more likely to affect the optical properties of NCs (i.e. the absorption and PL). The acoustic phonons represent a strain in the crystal that has pronounced effect on thermal properties like thermal conductivity and the mobility. The anomalous temperature dependence of bandgap energy in these materials is explained via using the Bose-Einstein two-oscillator model which also provided additional

insight about the vibrational dynamics in $CsPbX_3$ NCs. Our results also show that bandgap of $CsPbBr_3$ and $CsPbI_3$ is renormalized due to the zero point motion of lead and halide oscillators. The red-shift of the NC PL peak energy results from relative contribution of Pb-like acoustic and X-like (X = Br, I) optical modes, with both opposing each other and also have a different temperature dependence on the phonon population.

Supporting Information

Supporting Information is available from the Wiley Online Library or from the author.

Data Availability

All the data used in the study are available from the corresponding author on request.

Acknowledgements

This work was supported by UK Engineering and Physical Sciences Research Council (EPSRC) grant EP/M015513/1.

Received: ((will be filled in by the editorial staff))
Revised: ((will be filled in by the editorial staff))
Published online: ((will be filled in by the editorial staff))

REFERENCES

[1] D. V. Talapin, J.-S Lee, M. V. Kovalenko, E. V. Shevchenko, *Chem. Rev.* **2010,** 110,389.

[2] R. Saran, R. J. Curry, *Nat. Photon.* **2016,** 10, 81.

[3] Y. Shirasaki, G. J. Supran, M. G. Bawendi, V. Bulovic, *Nat. Photon.* **2013,** 7, 13.

[4] L. Protesescu, S. Yakunin, M. I. Bodnarchuk, F. Krieg, R. Caputo, C. H. Hendon, R. X. Yang, A.Walsh, M. V. Kovalenko, *Nano Lett.* **2015,** 15, 3692.

[5] J. Song, J. Li, X. Li, L. Xu, Y. Dong, H. Zeng, *Adv. Mater.* **2015,** 27, 7162.

[6] S.Yakunin, L. Protesescu, F. Krieg, M. I. Bodnarchuk, G. Nedelcu, M. Humer, G. De Luca, M Fiebig, W. Heiss, M. V. Kovalenko, *Nat. Commun.* **2015,** 6, 8056.

[7] J. A. Castañeda, G. Nagamine, E. Yassitepe, L. G. Bonato, O. Voznyy, S. Hoogland, A. F. Nogueira, E. H. Sargent, C.H.B. Cruz, L.A. Padilha, *ACS Nano* **2016,** 10, 8603.

[8] N. S. Makarov, S. Guo, O. Isaienko, W. Liu, I. Robel, V. I. Klimov, *Nano Lett.* **2016,** 16, 2349.

[9] G. Rainò, G.Nedelcu, L. Protesescu, M. I. Bodnarchuk, M. V. Kovalenko, R. F. Mahrt, T. Stöferle, *ACS Nano* **2016,** 10, 2485.

[10] K. Wu, A. Bera, C. Ma, Y. Du, Y.Yang, L. Li, T. Wu, *Phys. Chem. Chem. Phys.* **2014,** 16, 22476.

[11] A. D. Wright, C.Verdi, R. L. Milot, G. E. Eperon, M. A. Perez-Osorio, H. J. Snaith, F. Giustino, M. B. Johnston, L. M. Herz, *Nat. Commun.* **2016,** 7, 11755.

[12] M. Sebastian, J. A. Peters, C. C. Stoumpos, J. Im, S. S. Kostina, Z. Liu, M. G. Kanatzidis, A. J. Freeman, B. W. Wessels, *Phys. Rev. B* **2015,** 92, 235210.

[13] H. He, Q.Yu, H. Li, J. Li, J. Si, Y. Jin, N. Wang, J. Wang, J. He, X. Wang, Y. Zhang, Z. Ye, *Nat. Commun.* **2016,** 7, 10896.

[14] R. L. Milot, G. E. Eperon, H. J. Snaith, M. B. Johnston, L. M. Herz, *Adv.Funct. Mater.* **2015,** 25, 6218.

[15] H.-H. Fang, R. Raissa, M. Abdu-Aguye, S. Adjokatse, G. R. Blake, J. Even, M.A. Loi, *Adv. Funct. Mater*. **2015,** 25, 2378.

[16] J. Dai, H. Zheng, C. Zhu, J. Lu, C. Xu, *J. Mater. Chem. C* **2016,** 4, 4408.

[17] M. I. Dar, G. Jacopin, S. Meloni, A. Mattoni, N. Arora, A. Boziki, S. M. Zakeeruddin, U. Rothlisberger, M. Grätzel, *Sci. Adv.* **2016,** 2, 1601156.

[18] H. Benisty, C. M. Sotomayor-Torrès, C. Weisbuch, *Phys. Rev. B* **1991,** 44, 10945.

[19] H. Benisty, *Phys. Rev. B* **1995,** 51, 13281.

[20] U. Bockelmann, G. Bastard, *Phys. Rev. B* **1990,** 42, 8947.

[21] T. Inoshita, H. Sakaki, *Phys. B: Condens. Matter* **1996,** 227, 373.

[22] D. Bozyigit, N. Yazdani, M.Yarema, O. Yarema, W. M. M. Lin, S. Volk, K. Vuttivorakulchai, M. Luisier, F. Juranyi, V. Wood, *Nature* **2016,** 531, 618.

[23] P. Han, G. Bester, *Phys. Rev. B* **2015,** 91, 085305.

[24] R. D. Schaller, J.M. Pietryga, S. V. Goupalov, M. A. Petruska, S. A. Ivanov, V. I. Klimov, *Phys. Rev. Lett.* **2005,** 95,196401.

[25] S. V. Kilina, D. S. Kilin, O.V. Prezhdo, *ACS Nano* **2009,** 3, 93.

[26] K. Heidrich, W. Schäfer, M. Schreiber, J. Söchtig, G. Trendel, J. Treusch, T. Grandke, H. J. Stolz, *Phys. Rev. B* **1981,** 24, 5642.

[27] D. Fröhlich, K. Heidrich, H. Künzel, G. Trendel, J. Treusch, *J. Lumin.* **1979,** 18, 385.

[28] G. Zohar, R. Baer, E. Rabani, *J. Phys. Chem. Lett.* **2013,** 4, 317.

[29] X. B. Zhang, T. Taliercio, S. Kolliakos, P. Lefebvre, *J. Phys.: Condens. Matter* **2001,** 13, 7053.

[30] S. Rudin, T. L. Reinecke, B. Segall, *Phys. Rev. B* **1990,** 42,11218.

[31] J. Lee, E. S. Koteles, M. O. Vassell, *Phys. Rev. B* **1986,** 33, 5512.

[32] Y. Chen, G. P. Kothiyal, J. Singh, P. K. Bhattacharya, *Superlattices Microstruct.* **1987,** 3, 657.

[33] A. K. Viswanath, J .I. Lee, D. Kim, C. R. Lee, J. Y. Leem, *Phys. Rev. B* **1998,** 58, 16333.

[34] R. Chen, D. Li, B. Liu, Z. Peng, G. G. Gurzadyan, Q. Xiong, H. Sun, *Nano Lett.* **2010,** 10, 4956.

[35] J. Tilchin, D. N. Dirin, G. I. Maikov, A. Sashchiuk, M. V. Kovalenko, E. Lifshitz, *ACS Nano* **2016,** 10, 6363.

[36] A. Buin, R. Comin, J. Xu, A. H. Ip, E. H. Sargent, *Chem. Mater.* **2015,** 27, 4405.

[37] H. D. Sun, T. Makino, N. T. Tuan, Y. Segawa, M. Kawasaki, A. Ohtomo, K. Tamura, H. Koinuma, *Appl. Phys. Lett.* **2001,** 78, 2464.

[38] A. D. Wright, C. Verdi, R. L. Milot, G. E. Eperon, M. A. Pérez-Osorio, H. J. Snaith, F. Giustino, M. B. Johnston, L. M. Herz, *Nat. Commun.* **2016,** 7, 11755.

[39] M. Sendner, P. K. Nayak, D. A. Egger, S. Beck, C. Muller, B. Epding, W. Kowalsky, L. Kronik, H. J. Snaith, A. Pucci, R. Lovrincic, *Mater. Horiz.* **2016,** 3, 613.

[40] D. M. Calistru, L. Mihut, S. Lefrant, I. Baltog, *J. Appl. Phys.* **1997,** 82, 5391.

[41] C. Carabatos-Nédelec, M. Oussaïd, K. Nitsch, *J. Raman Spectrosc.* **2003,** 34, 388.

[42] M. I. Cohen, K. F. Young, T. T. Chang, W. S Brower, *J. Applied Phys.* **1971,** 42, 5267.

[43] J. A. Cape, R. L. White, R. S. Feigelson, *J. Applied Phys.* **1969,** 40, 5001.

[44] C. E. P. Villegas, A. R. Rocha, A. Marini, *Nano Lett.* **2016,** 16, 5095.

[45] C. Yu, Z. Chen, J. J. Wang, W. Pfenninger, N. Vockic, J. T. Kenney, K. Shum, K. *J. Appl. Phys.* **2011,** 110,063526.

[46] H. J. Lian, A. Yang, M. L. W. Thewalt, R. Lauck, M. Cardona, M. *Phys. Rev. B* **2006,** 73, 233202.

[47] P. Dey, J. Paul, J. Bylsma, D. Karaiskaj, J. M. Luther, M.C.. Beard, A. H. Romero, A. H. *Solid State Commun.* **2013,** 165, 49.

[48] M. N. Nordin, L. Juerong, S. K. Clowes, R. J. Curry, *Nanotechnology* **2012,** 23, (27), 275701.

[49] A. Göbel, T. Ruf, M. Cardona, C. T. Lin, J. Wrzesinski, M. Steube, K. Reimann, J.C. Merle, M. Joucla, *Phys. Rev. B* **1998,** 57,15183.

[50] Y.P. Varshni, *Physica* **1967,** 34,149.

[51] K.P. O'Donnell, X. Chen, X. *Appl. Phys. Lett.* **1991,** 58, 2924.

[52] R. Pässler, *J. Appl. Phys.* **2001,** 89, 6235.

[53] L.-Y. Huang, W. R. L. Lambrecht, *Phys. Rev. B* **2013,** 88, 165203.

[54] M. Cardona, M. *Phys. status solidi (a)* **2001,** 188, 1209.

[55] J. Bhosale, A. K. Ramdas, A. Burger, A. Muñoz, A. H. Romero, M. Cardona, R. Lauck, R. K. Kremer, *Phys. Rev. B* **2012,** 86,195208.

[56] H.Y. Fan, *Phys. Rev.* **1951,** 82, 900.

[57] P.B. Allen, M. Cardona, *Phys. Rev. B* **1981,** 23, 1495.

[58] S. Gopalan, P. Lautenschlager, M. Cardona, M. *Phys. Rev. B* **1987,** 35, 5577.

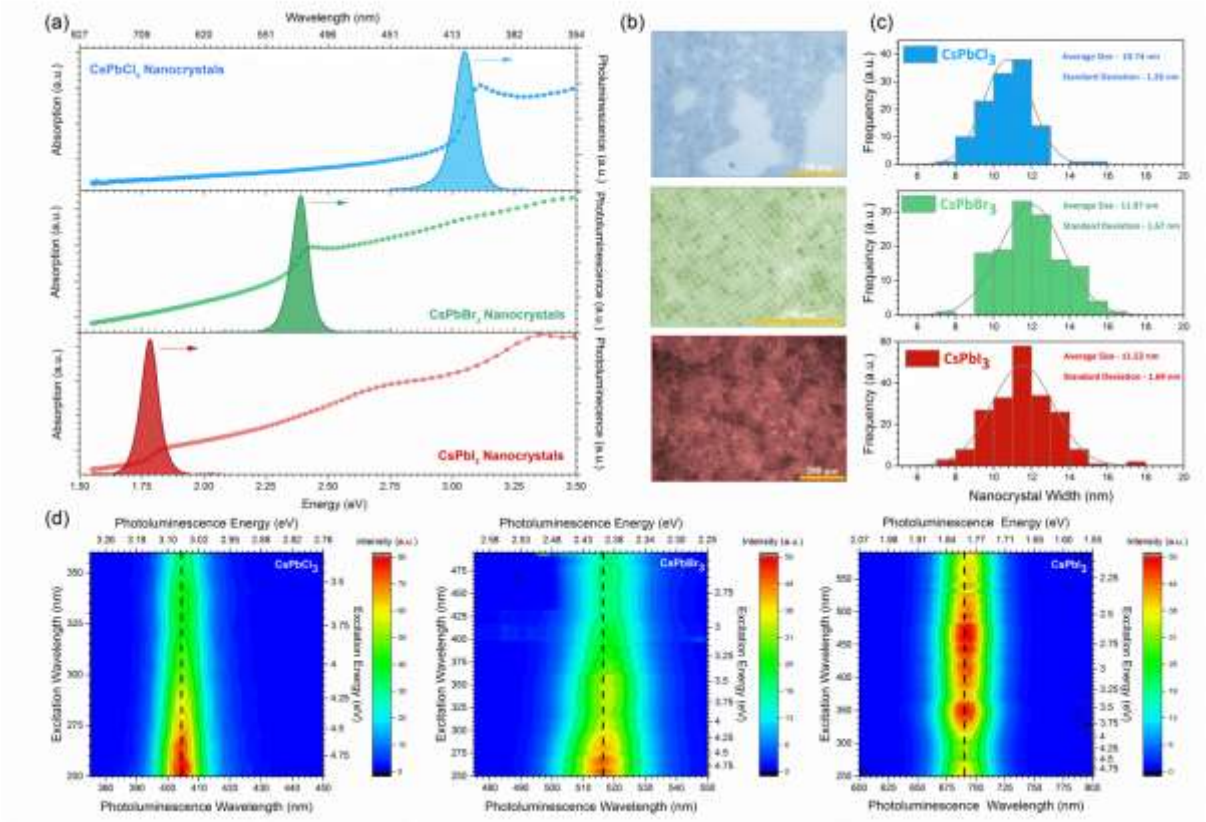

Figure 1. $CsPbX_3$ (X = Cl, Br, I) NC optical absorption, PL, size distribution and PLE. a) Room temperature absorption and PL of as synthesized oleic acid (oleylamine) ligated $CsPbX_3$ NCs. It can be seen that by selection of the halide ion the absorption and PL emission of the NCs can be strongly modified from the blue (emitting at ~3.04 eV) for Cl, to green (emitting at ~2.38 eV) for Br, to the red (emitting at ~1.78 eV) for I. Corresponding PL full widths at half maximum (FWHM) of ~101 meV, ~86 meV and ~87 meV are found. In each case a relatively small Stoke's shift is observed between the PL emission and absorption (~50 meV, ~23 meV and ~41 meV for Cl, Br and I NCs respectively). b) Transmission electron microscopy (TEM) images of cubic shaped $CsPbX_3$ perovskite NCs. Enlarged greyscale TEM images of the respective NCs are shown in supporting information figure S1, S2 and S3 c). Size distribution of the cubic $CsPbX_3$ NCs used in this study have average width (*W*) of ~10.7 nm, ~12.0 nm and ~11.5 nm for Cl, Br and I based crystals respectively and are therefore close to the bulk exciton Bohr diameter for Cl and Br, and are in the strong confinement regime for I. d) 2D contour plots of the PLE spectra of $CsPbX_3$ NCs showing the effect of excitation energy on both PL emission energy and intensity. The black dotted line, centered on the emission peak when exciting at 250 nm, enables the small shift of the PL emission to be observed as the excitation energy is reduced.

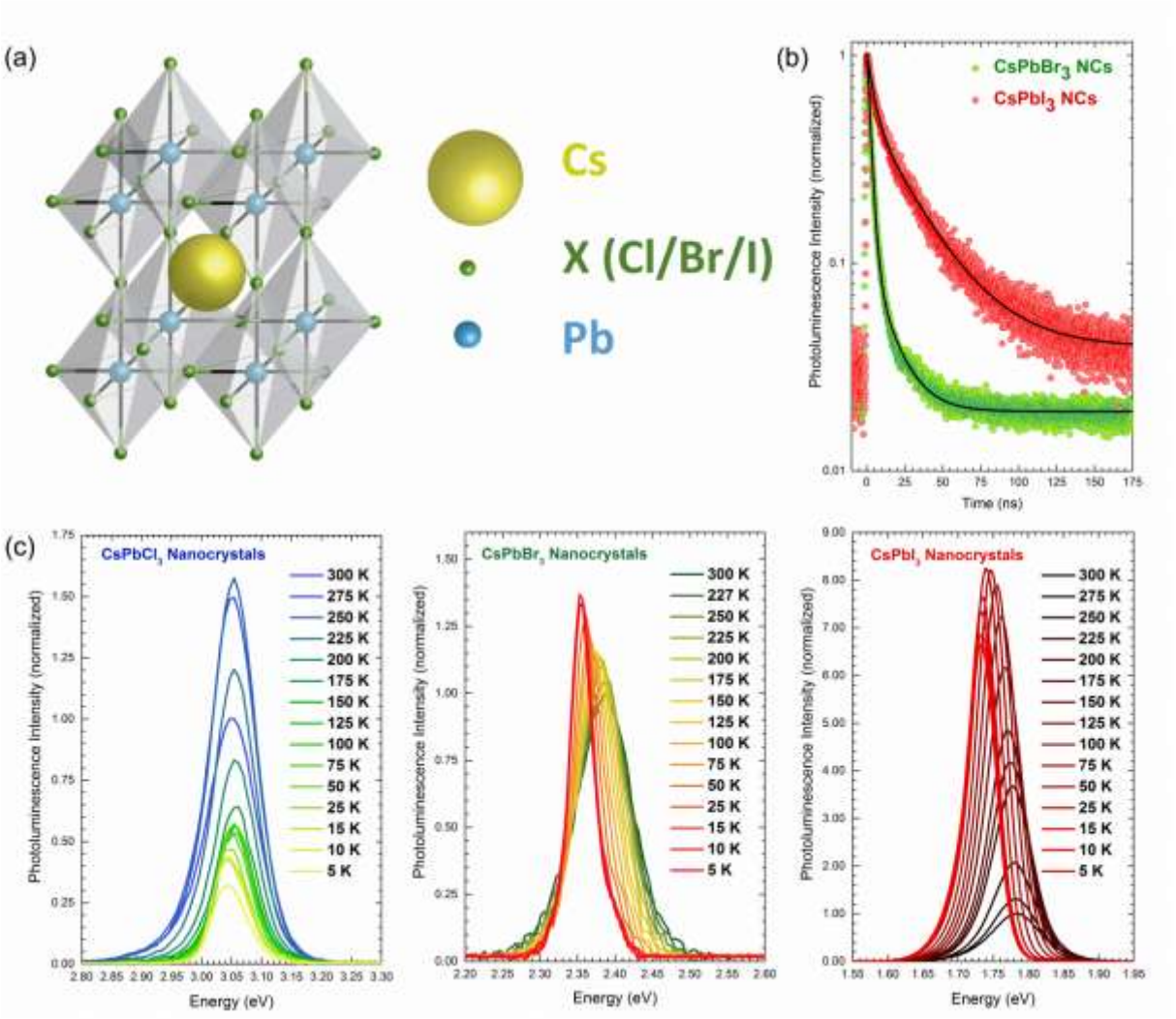

Figure 2. $CsPbX_3$ NC crystal structure, PL lifetime decay and the temperature dependence of the NC PL. a) A schematic of the crystal structure of $CsPbX_3$. The inorganic Cs^{+1} cations occupy position A (yellow), Pb^{+2} cations are located at position B (blue) and the halogen anions ($Cl^-/Br^-/I^-$) occupy position X (green) in the perovskite crystal. b) Transient PL decay curves of $CsPbBr_3$ and $CsPbI_3$ NCs and fitting using a bi-exponential decay function (black lines). c) PL emission spectra of $CsPbX_3$ NCs measured over the temperature range of 300 K to 5 K, normalized to the peak emission intensity at 300 K.

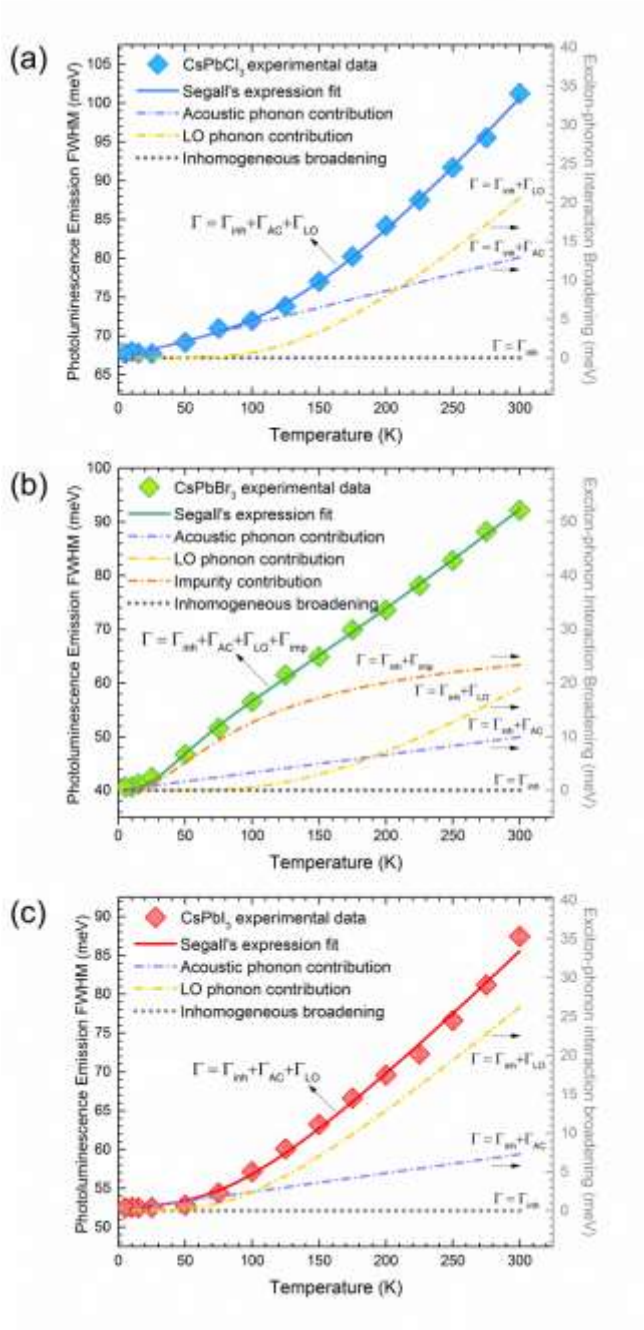

Figure 3. Exciton-phonon interactions in $CsPbX_3$ NCs. a-c) The temperature dependence of the PL FWHM for $CsPbX_3$ NCs. The coloured squares are the experimental data fitted using Segall's expression (solid line). The temperature dependence of the PL exciton linewidth broadening arising from acoustic phonon interaction $\Gamma(T) = \Gamma_{inh} + \Gamma_{AC}$ (violet dash-dot line), LO phonon interaction $\Gamma(T) = \Gamma_{inh} + \Gamma_{LO}$ (yellow dash-dot line), inhomogeneous broadening term $\Gamma(T) = \Gamma_{inh}$ (horizontal grey dotted line) and due to the presence of impurities $\Gamma(T) = \Gamma_{inh} + \Gamma_{imp}$ (in the case of $CsPbBr_3$ NCs only, orange dash-dot line in (b)) is also shown in the respective figure for each NCs type.

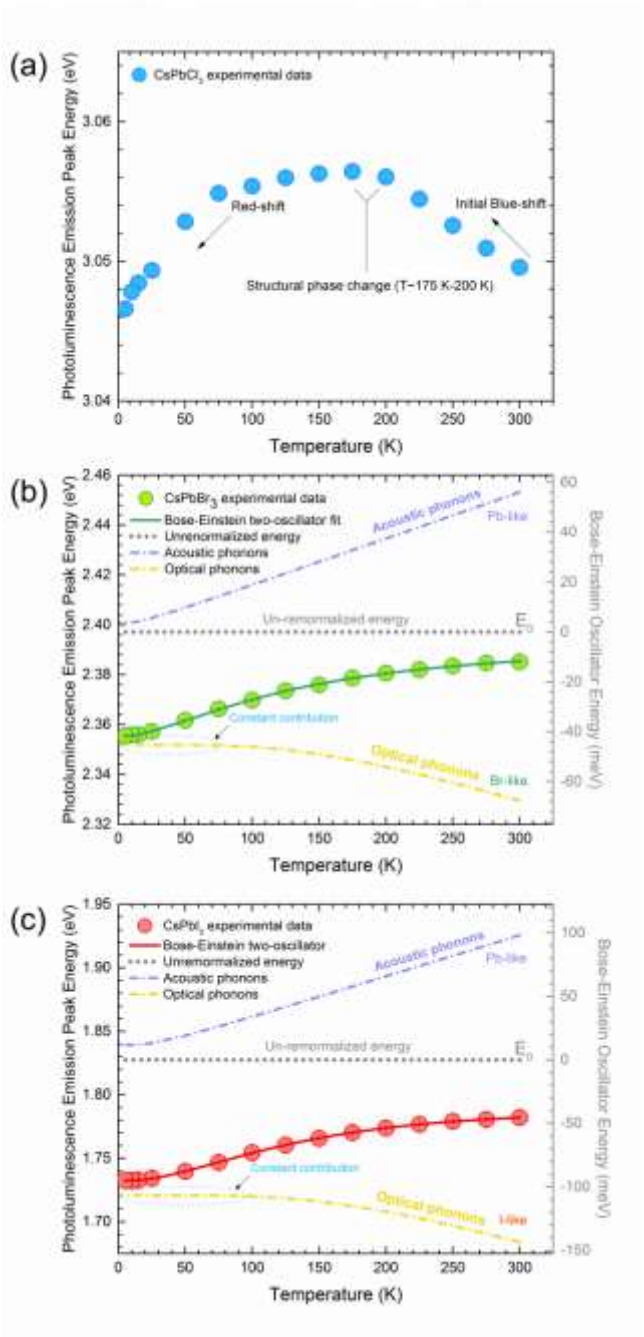

Figure 4. Exciton-phonon interactions in $CsPbX_3$ NCs. a-c) The temperature dependence of the PL peak energy of $CsPbX_3$ NCs. The coloured circles are the experimental data. As seen in (a) $CsPbCl_3$ NCs display an initial blue shift followed by a red-shift after undergoing a structural phase change in the crystal at T ~175 K – 200 K. In (b) and (c) the experimental data is fitted using a Bose-Einstein two-oscillator model for $CsPbBr_3$ and $CsPBI_3$ NCs. The horizontal line (grey dotted line) is the unrenormalized bandgap energy (left axis). The relative contribution to the shift in energy arising from Pb-like acoustic and X-like optical phonons is shown in (b) and (c) (right axis).

Table 1. Parameters derived via fitting the PL FWHM temperature dependence with Segall's expression.

Perovskite NCs	Γ_{inh} [meV]	γ_{AC} [μeV/K]	γ_{LO} [meV]	E_{LO} [meV]
$CsPbCl_3$	67.18±0.27	43.14±5.50	87.22±14.9	42.82±4.45
$CsPbBr_3$	40.04 ±0.45	33.05±11.07	86.72±31.40	44.35±10.19
$CsPbI_3$	52.12±0.71	24.17±21.96	46.13±11.10	26.25±6.96

Table 2. Parameters derived via fitting the PL peak energy temperature dependence using a Bose-Einstein two-oscillator model.

Perovskite NCs	E_0 [meV]	A_{opt}	ω_{opt} [meV]	A_{ac}	ω_{ac} [meV]
$CsPbBr_3$	2397.13±4.80	-(0.30±0.05)	41.87±3.61	(0.005±0.002)	3.42±0.06
$CsPbI_3$	1827.49±6.13	-(1.34±0.12)	49.53±2.14	(0.030±0.004)	6.27±0.04